JOURNAL OF MATERIALS SCIENCE **34** (1999) 3533–3544

X-ray photoelectron spectroscopy and electrical properties studies of La_2O_3-doped strontium titanate ceramics prepared by sol-precipitation method

WEIN-DUO YANG
Department of Chemical Engineering, National Kaohsiung Institute of Technology, Kaohsiung 80807, Taiwan
E-mail: ted@nkitch.nkit.edu.tw

X-ray photoelectron spectroscopy has been used to investigate the existence of Ti^{3+} on the surface of La_2O_3-doped strontium titanate and to determine its surface characteristics. The surfaces, having Sr/Ti ratios significantly varying from the stoichiometric ratio, revealed the presence of carbon and suggested the presence of hydroxyl groups on the surface, whose concentration largely decreased in the bulk. Ti^{3+} species existed as a function of the sintering conditions and were detected on the surface of (La, Sr)TiO_3 sintered in air or in N_2 by natural cooling. These samples had a lower electrical resistivity, especially when sintered in a N_2 atmosphere. The surfaces of air oxidized $SrTiO_3$ and quenched from high temperature contained no detectable amount of Ti^{3+}, resulting in higher resistivity. However, the N_2-sintered samples were dark blue in color and exhibited lower resistivity, semiconductivity, and lower valence oxidation state Ti existed when sintered above 1350 °C. © *1999 Kluwer Academic Publishers*

1. Introduction

The titanyl acylate precursor made from chelating acetic acid with titanium alkoxide, precipitated in a strong alkaline solution and reacted with alkali earth metal ions, Sr^{2+}, to yield strontium titanate above room temperature [1–3]. One can obtain a powder of uniform chemical composition, and this route of preparation is valuable when only small amounts of the dopant have to be dispersed homogeneously [4]. Kao and Yang [5] have prepared ultrafine $SrTiO_3$ powder of 0.04–0.05 μm particle size by modifying the above sol-precipitate method, and the powder sintered for four hours at 1300 °C was very dense, about 98% of its theoretical density.

Strontium titanate is a ceramic used in electronics. Applying its semiconducting properties, it is being widely used for capacitors [6–8] and photoelectrodes [9–11]. The semiconducting behavior is achieved at room temperature by reduction or by doping with La^{3+} etc. [12, 13]. Frederikse *et al.* [14] indicated that incorporation of La^{3+}-ions in strontium titanate results in $La_x^{3+}Sr_{1-x}^{2+}Ti_x^{3+}Ti_{1-x}^{4+}O_3^{2-}$ under oxidizing conditions. The substitution of Sr^{2+} by the La^{3+}-ion in the crystal lattice is compensated by the formation of Ti^{3+} ions. As the lanthanum content is increased, the amount of Ti^{3+} should also increases, resulting in a higher conductivity of the material [15].

X-ray photoelectron spectroscopy (XPS) can be used to study the chemical state and abundance of the constituent elements on the surface. Recently, a series of XPS studies were reported by scholars. Henrich *et al.* [16] discussed the effect of surface defects on the electronic structure and reactivity of $SrTiO_3$ and TiO_2. They concluded that the reactivity of these surfaces are related to the presence of such surface defects. Furthermore, S. Ferrer *et al.* [17] used UPS and XPS to study the chemisorption of O_2, H_2 and H_2O on reduced and stoichiometric $SrTiO_3$ (111) surfaces. They found that a high concentration of Ti^{3+} could be detected by XPS on the surface of the reduced oxide, but the stoichiometric $SrTiO_3$ surface showed no detectable amounts of Ti^{3+}. Comparison of these two extremes of surface chemical activities for the reduced and stoichiometric oxides clarifies the roles of Ti^{3+} and surface hydroxylation during the photochemical dissociation of water. Nagarkar *et al.* [18] studied the reoxidation kinetics of both mechanically and chemically polished and freshly fractured $SrTiO_3$ surfaces. Both adsorbed hydroxyl and carbonate O 1s levels, showing that hydroxyl adsorption occurs very rapidly. Furthermore, Carley *et al.* [19] discussed the methodology of extracting informatation on the presence of Ti^{2+}, Ti^{3+} and Ti^{4+} from an analysis of the Ti (2p) spectra observed during the formation of thin oxide films.

However, the influence of Ti^{3+} on the bulk's electrical properties has not been reported. In this work, we investigated the surface of a sol-precipitated La_2O_3-doped $SiTiO_3$ ceramic sintered in air and in N_2 using

XPS. Two different cooling methods were used: natural cooling in the furnace and quenching from high temperatures. The experimental data for materials sintered in a N_2 atmosphere suggest that the Ti^{3+} species existing on the surface is responsible for the ceramic's semiconductive properties.

2. Experimental

$(La_{0.005},Sr_{0.995})TiO_3$ powder was prepared by the sol-precipitation method using acetic acid to chelate titanium isopropoxide. The preparatory procedures are detailed in reference [20]. The bulks made from the above powder were being compacted at 110 MPa; three different sintering methods were used in this study. The pressed discs were sintered at temperatures between 1300 and 1450 °C for two hours in either air or N_2. And the above bulks were cooled to room temperature in the furnace under the respective atmosphere. To investigate the existence of Ti^{3+} on the surface, we chose a $(La,Sr)TiO_3$ bulk which was sintered in air and quenched into water from high temperature. We refer in this article to the three kinds of sintered samples as air, N_2 and quench types.

Surface analysis of the titanate samples was carried out using a V.G. Instruments X-ray photoelectron spectrometer. MgK_α radiation was used as the X-ray source and the photoelectron peaks from the samples were numerically fitted using Lorentzian curves with an integral background subtraction and analyzed at an angle of 45 ° to the surface. The adventitious C 1s signal at 284.6 eV was used to calibrate the charge-shifted energy scale. The X-ray spot size was 600 mm and the resolution was about 0.8 eV always, the spectra represent original experimental data recorded to an accuracy of 0.2 eV. In addition, the spectra were deconvoluted for chemical identification using 100% Gaussian peaks.

For measurement of the electrical properties, the sintered bulks were coated with conductive silver paste as electrodes. The electrodes, after coating at 700 °C, were used to measure the A.C. electrical resistivity and dielectric constant with a HP LCR analyzer 4284A at room temperature.

3. Results and discussion

Using X-ray diffraction, the (110) plane and (200) plane of the bulks sintered at 1450 °C were detected. They present two principal reflections of the cubic perovskite structure of $SrTiO_3$ (not shown). Though other phases, such as TiO_2 and Magnéli phases (Ti_3O_5, $Ti_4O_7, \ldots, Ti_nO_{2n-1}$), also existed in same bulks, combined XRD and XPS measurements showed that the surfaces contained mainly $SrTiO_3$.

3.1. Survey scan of the surfaces

Typical XPS surveys of 0–1000 eV for $(La,Sr)TiO_3$ surfaces are shown in Fig. 1, revealing only the existence of Sr, Ti, O, and C signals in the samples. The carbon contamination largely decreased after ion sputtering, suggesting that it was produced by atmospheric carbon compounds when the surface was exposed to air.

The bulks were sintered using the above three methods at 1450 °C, and sputtered with Ar for 15 minutes. The atomic percents of La, Ti, Sr, and O on the surface, calculated from the corresponding photoelectron peak area sensitivity factor corrections are listed in Table I.

The results show that the unpolished surfaces contained a lot more carbon and oxygen than the polished

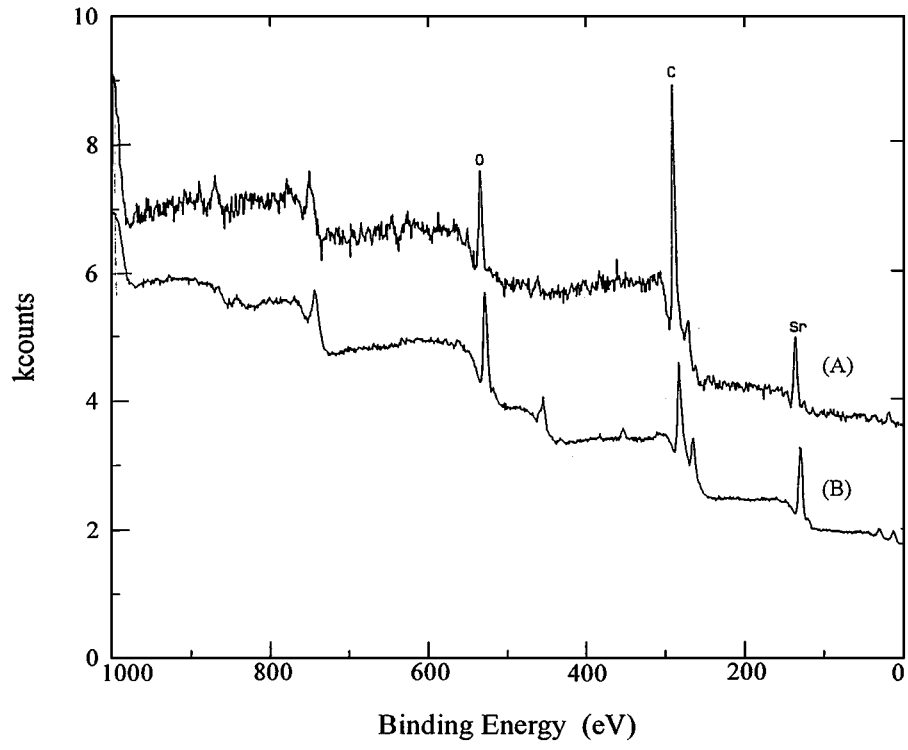

Figure 1 XPS survey of $(La,Sr)TiO_3$ surfaces: (A) sample sintered in air at 1450 °C for 2 h without sputting and (B) sample sintered in air at 1450 °C for 2 h and sputtered by Ar for 15 min.

TABLE I Surface stoichiometries (XPS) in percent for La-doped $SrTiO_3$ surface

Samples	La(3d)	O(1s)	Ti(2p)	C(1s)	Sr(3d)	Ti/Sr	O/Sr
Air unsputtered	0.5	26.7	5.9	56.1	10.8	0.5	2.5
Air sputtered	1.3	34.3	20.3	32.7	11.5	1.7	3.1
N_2 unsputtered	0.2	23.1	3.3	60.7	12.7	0.3	1.8
N_2 sputtered	3.2	41.8	5.9	35.8	13.3	0.5	3.1
Quenched unsputtered	0.5	52.4	2.1	40.5	5.5	0.4	9.5
Quenched sputtered	0.3	18.9	4.8	70.6	5.4	0.9	3.5

surfaces. The excess carbon on the unpolished surface is assumed to be carbonate (Young *et al.* [21]). It was shown that $SrTiO_3$ has a strong tendency to chemisorb carbon dioxide, and the excess oxygen on the bulk's surface is attributed to surface sensitivity of adsorbed H_2O.

Although the bulks' compositions were very close to stoichiometric, mesured by AA, the surfaces were found to have Ti/Sr ratios that varied significantly from the stoichiometric ratio. The Ti/Sr, and O/Sr ratios of the quenched surface are shown in Table I. These ratios reveal that the surface of the quenched sample contains relatively more oxygen than the other surfaces. This can be explained by the fact that oxygen can easily diffuse to the surface when $SrTiO_3$ is quenched from high temperature.

3.2. Detailed XPS surface analysis

3.2.1. Ti surface analysis

The asymmetric Ti 2p peaks of surfaces sintered at 1450 °C are shown in Fig. 2. Fig. 2A shows that the Ti core level of the air-sintered $SrTiO_3$ surface simulated by Gaussians resolves into three components. One peak at the highest binding energy, centered at 459.5 eV, is attributed to TiO_2 [22, 23]. The second peak, centered at 457.8 eV, with a full-width at half maximum (FWHM) of 1.6 eV, is assigned to the Ti^{4+} $2p_{3/2}$. The peak position and line splitting are in accordance with the values reported for $SrTiO_3$ [18]. A third peak is centered at the binding energy of 455.0 eV, with a FWHM of 1.2 eV, at 2.8 eV from the Ti $2p_{3/2}$ peak. The presence of lower oxidation states would be expected to result in additional contributions on the low binding energy sides of the 2p peak. The binding energy of the third peak is identified as Ti^{2+} $2p_{3/2}$ in TiO [19]. The area ratio of these three peaks is estimated as 2 : 90 : 8, suggesting that the Ti peak of $SrTiO_3$ is greater than that of lower oxidation state titanium.

Fig. 2B shows that the Ti 2p line of the N_2-sintered titanate surfaces resolves into three peaks. The first one, at 459.3 eV, with a FWHM of 1.8 eV, having a higher binding energy than Ti $2p_{3/2}$ of $SrTiO_3$ is attributed to TiO_2. And the second one, centered at 457.4 eV, is attributed to $SrTiO_3$, having a FWHM of 1.3 eV. The last one, positioned at 456.1 eV, with a FWHM of 1.2 eV, is attributed to Ti_2O_3. According to the peak areas the ratio of TiO_2, $SrTiO_3$, and Ti_2O_3 is calculated to be 46 : 36 : 18.

To understand the existence of surface Ti^{3+} at high temperatures, we did an experiment on an air-fired (La,Sr)TiO_3, quenched into water from 1450 °C. The corresponding XPS spectrum is shown in Fig. 2C. TiO_2 and $SrTiO_3$ are detected on the surface with mol fractions of 16% and 84%, respectively. Since there is no visible peak emerging from the background in the 1 eV region, this surface has no detectable concentration of lower oxidation state titanium (Ti^{3+}). The surface XPS studies indicated that the N_2-sintered bulk contained more lower oxidation state Ti (Ti^{3+}).

3.2.2. Sr surface analysis

The asymmetric Sr 3d peak shown in Fig. 3 is consistent with those reported for the Sr^{2+} states [18]. This Sr core level of the air-sintered surface can be split into two components by Gaussian analysis as shown in Fig. 3A. The peak having a higher binding energy at 134.3 eV, with a FWHM of 1.2 eV, is identified as the Sr $3d_{3/2}$ peak of $SrTiO_3$. The other peak on the lower energy side is centered at 132.6 eV, with a FWHM of 1.8 eV, and assigned as the Sr $3d_{5/2}$ peak of $SrTiO_3$. The binding energies of the Sr 3d peaks were consistent with those reported for strontium ions in Sr^{2+} states [24–26].

Fig. 3B shows the Sr 3d binding energy of an N_2-sintered surface. The Sr 3d signal displayed peaks at 133.8 and 132.2 eV, showing a slight change in line shape with respect to the surface Sr 3d peak shown in Fig. 3A. However, these peak positions, line shapes and line splittings are also in accordance with the values reported for $SrTiO_3$ in the literature [21]. However, an additional peak centered at 135.6 eV, which suggests the higher binding energy peak with a FWHM of 1.3 eV, to be SrO. The peak (peak A) is in accordance with the studies of Young *et al.* [21], who reported Sr 3d spectra for SrO pellets, and the Sr 3d peaks were identified by deconvolution to be at binding energies of about 1.4 eV higher than that of the Sr $3d_{3/2}$ in $SrTiO_3$.

Additionally, similar spectra were obtained from the quenched samples and are shown in Fig. 3C. It suggests that the sample surface contained less C (1s), and the peak having a higher binding energy centered at 135.9 eV with a FWHM of 1.3 eV, might be attributed to SrO [24]. The area percentage of this peak is estimated to be 5%. The energy separation between the Sr $3d_{5/2}$ and Sr $3d_{3/2}$ peaks of $SrTiO_3$ is also shown in this figure. The two main peaks were well defined with the same FWHM of 1.7 eV.

3.2.3. Oxygen surface XPS analysis

Fig. 4 shows the binding energies of O 1s spectra for (La,Sr)TiO_3 surfaces as a function of the different sintering conditions. Fig. 4A shows the O 1s spectrum

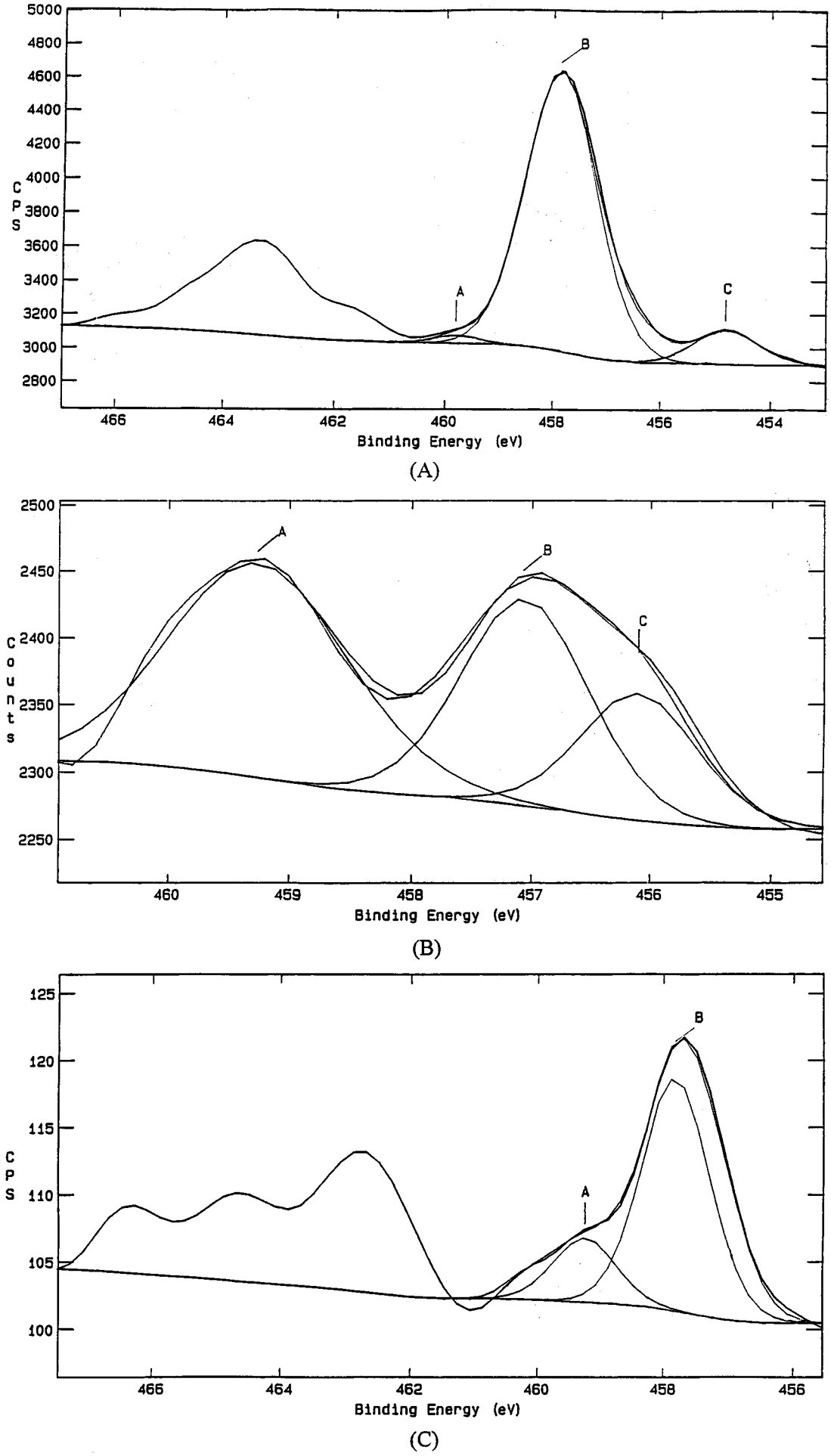

Figure 2 Ti 2p spectra for the unsputtered samples sintered at 1450 °C: (A) sintered in air, (B) sintered in N_2, and (C) the quenched sample.

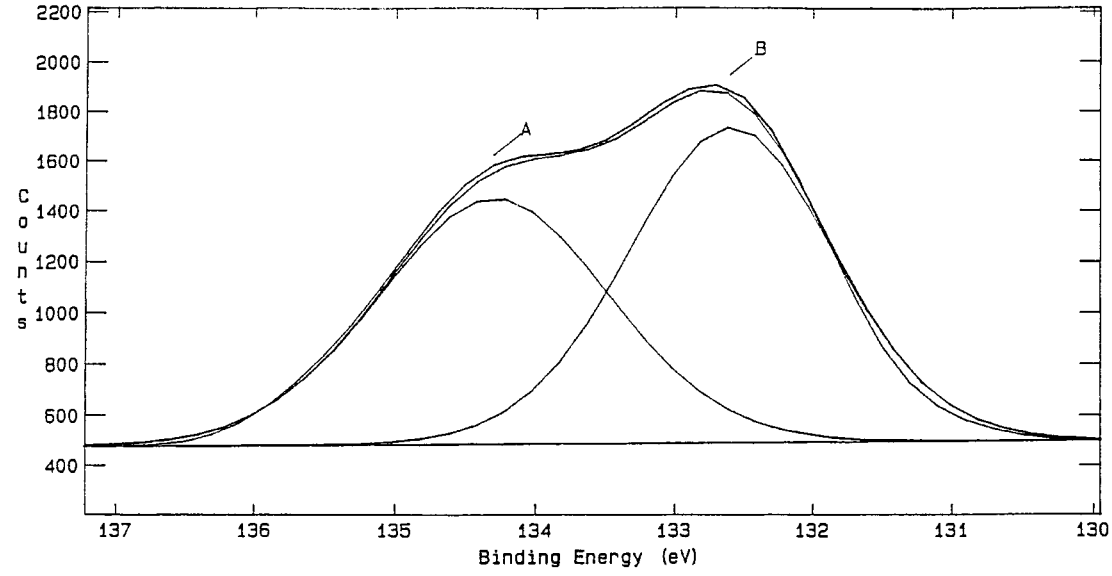

(A)

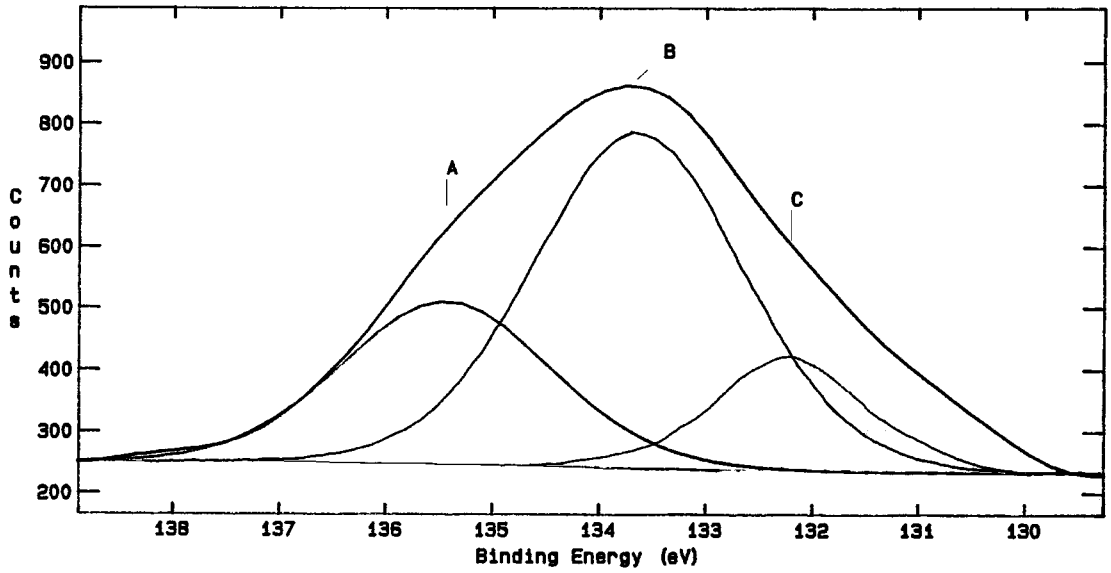

(B)

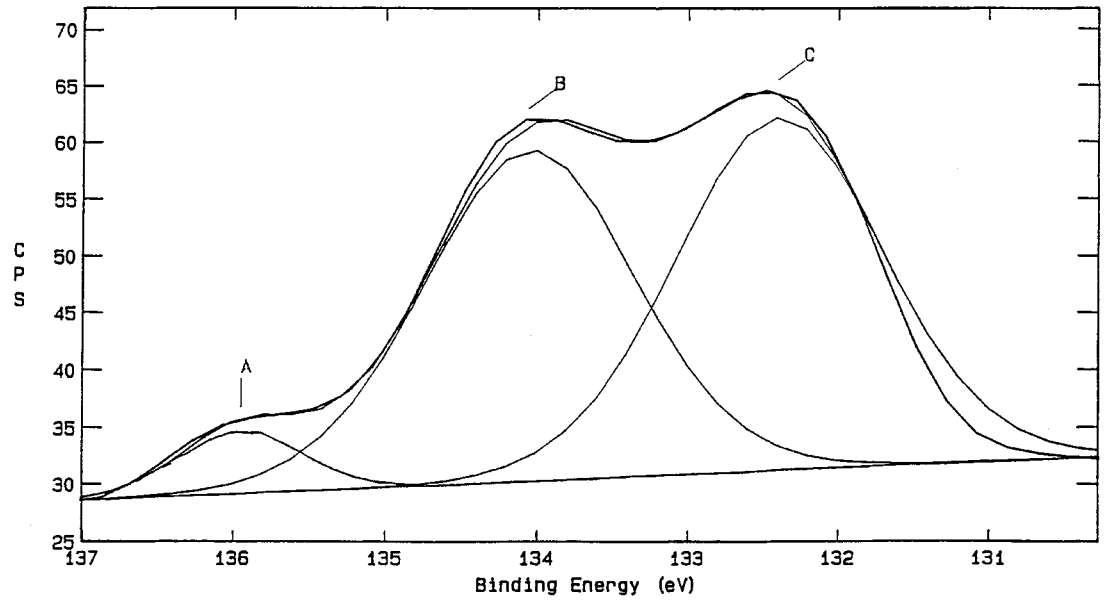

(C)

Figure 3 Sr $3d_{5/2}$ and $3d_{3/2}$ peaks for bulks sintered at 1450 °C: (A) sintered in air, (B) sintered in N_2, and (C) the quenched sample.

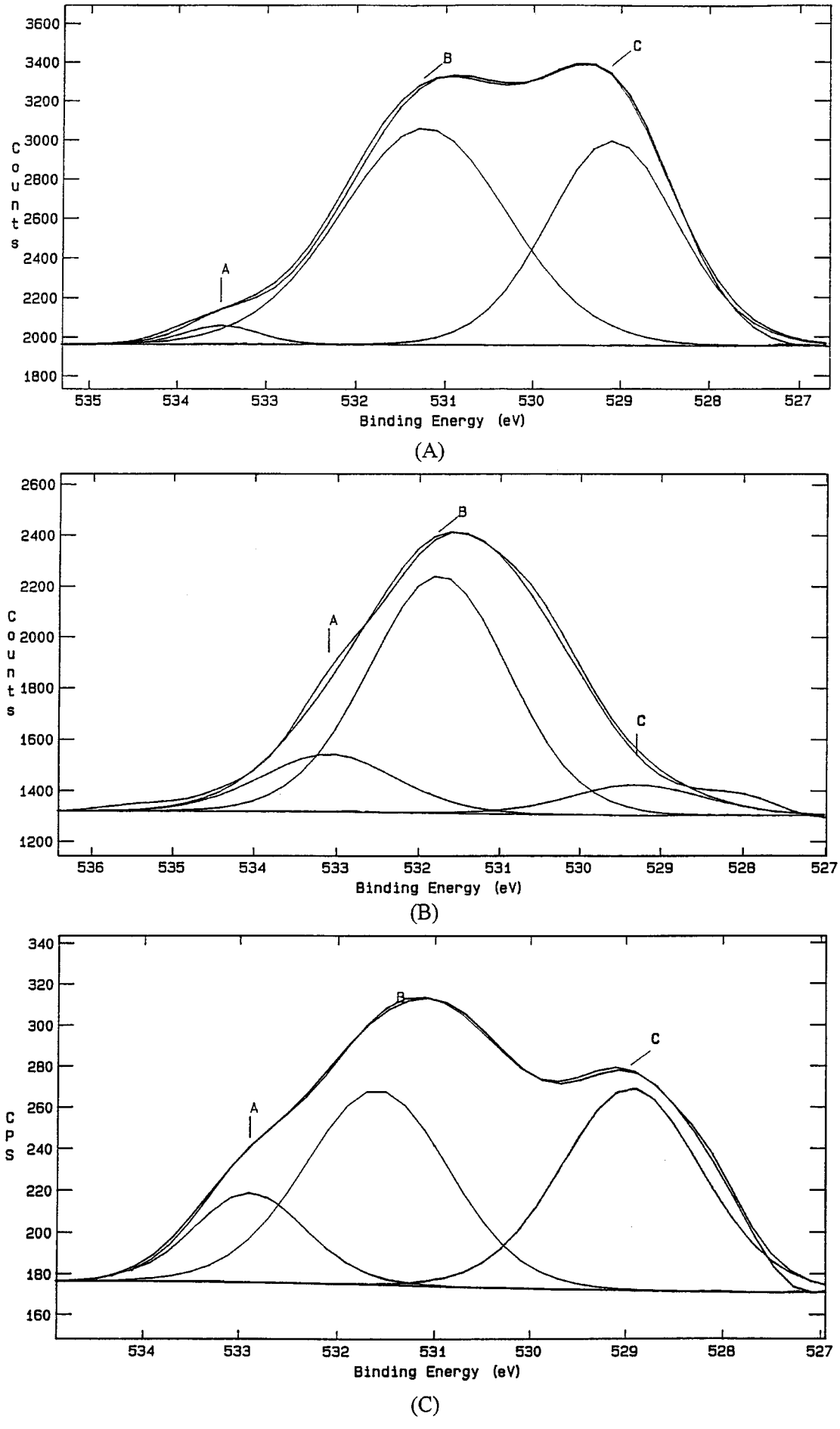

Figure 4 Oxygen 1s spectra for La-doped $SrTiO_3$: (A) sintered in air at 1450 °C for 2 h, (B) sintered in N_2 at 1450 °C for 2 h, and (C) sintered in air at 1450 °C for 2 h and quenched to room temperature.

for the $SrTiO_3$ oxidized in air. The O 1s spectrum for $SrTiO_3$ resolves into three peaks centered at 529.3, 531.6 and 533.4 eV, respectively. The main peaks are the ones at 531.6 and 533.4 eV. Fig. 4B shows a spectrum for N_2-sintered $SrTiO_3$. It displays peaks similar to the ones of Fig. 4A of an air-oxidized surface, except that the area of the peak centered at 531.8 eV is larger than the area of the peak centered at 529.3 eV.

The O 1s binding energies of a quenched surface are shown in Fig. 4C. This shows resolution of binding energies into three peaks, similar to those seen in Fig. 4A; the first peaks of Fig. 4A, B and C are centered at 529.3, 529.3, and 529.0 eV, respectively, suggesting titanate oxygen. These results are in good agreement with the air-oxidized fracture surface of $SrTiO_3$ reported by Nagarkar *et al.* [18].

Both the surfaces of air-sintered and quenched samples contain a large amount of the O 1s species (centered about 529.3 eV), revealing that $SrTiO_3$ is the main component of these surfaces. This is also in good agreement with the Ti XPS analysis described above. On the contrary, the N_2-sintered surface, probably due to the lack of oxygen, contains lower valence oxidation state titanium, such as Ti^{3+}. $SrTiO_3$ is not the main component of the surface, and therefore it contains less O 1s of $SrTiO_3$ centered at 529.3 eV.

The second oxygen peak in Fig. 4B at a binding energy of 531.6 eV, about 2.3 eV higher than the titanate oxygen peak, is a big peak. Knotek [27] revealed that high levels of contaminant hydroxyl species exist on $SrTiO_3$ surfaces, were associated primarily with titanium rather than strontium cations. Furthermore, the results of the XPS study of Ti are shown in Fig. 2. Fig. 2B shows that the surface of the N_2-sintered bulk contains a higher percentage of Ti bonded in various TiO_x-structures and relatively less Ti bonded as $SrTiO_3$ compared to the air-sintered sample. That means the overall percentage of Ti-ions on the surface of this sample is higher. The hydroxyl species is preferable bond to Ti. It explains the big peak at 531.6 eV (Fig. 4B, peak B), represents surface-adsorbed hydroxyl species.

A third oxygen peak is seen at a binding energy of 533.4 eV, about 4.1 eV higher than the titanate oxygen peak. This peak is thought to be related to a surface carbonate species [25]. Perhaps, SrO is a basic oxide and shows a strong tendency to chemisorb carbon dioxide and water vapor. The peak near 533.4 eV of the air-sintered sample greatly decreased (not shown) after Ar-sputtering. The survey scan (Fig. 1B), also shows that the carbon content greatly decreased after Ar-sputtering, indicating that results for the air- sintered $SrTiO_3$ are consistent with this interpretation.

3.2.4. Ti depth profile

The three bulks sintered at 1450 °C were sputtered with Ar for 15 minutes, and the corresponding XPS analyses of the Ti 2p binding energies are shown in Fig. 5. As shown above in Fig. 2A, the air-sintered unpolished sample contains lower valence Ti at a binding energy of 455.0 eV. Ti^{3+} amounts to 8 at % of the sample. Because of the similarity of the ionic radii of stable trivalent lanthanum and Sr^{2+} the La^{3+} ion can be expected to be incorporated at Sr sites. To achieve electrical neutrality the substitution of strontium by lanthanum is compensated by the creation of Ti^{3+}-ions. Fig. 5A shows the Ar-sputtered air-sintered surface. The atomic percentage of Ti 3p at 456.2 eV decreases and is compensated by the existence of Ti 3p binding energy at 459.2 eV with a mol fraction of 9%. The binding energy of 459.2 eV is higher than the binding energy of $SrTiO_3$ at 457.8 eV, and was assigned to the character of Ti^{4+} in the TiO_2. From this observation, one postulated that the surface contains relatively more Ti^{3+} (Ti_2O_3) than the inner profile material which is rich in TiO_2. Fujimoto *et al.* [28] used HRTEM and SEM to reveal Ti_nO_{2n-1} Magnéli phases (Ti_4O_7, Ti_5O_9 and others). The Magnéli phases exist at the multiple grain junctions in $SrTiO_3$. We suppose that Magnéli phases were formed by complexes of TiO_2 and Ti_2O_3 at the grain boundary inside of the bulk.

The Ar-sputtered N_2-sintered surface contains less Ti^{3+} located at 455.8 eV (shown in Fig. 5B). This shift agrees quantitatively with previously reported data on titanium suboxides [29]. And the TiO_2 had an assigned peak centered at 460.0 eV making up 12.2%. Compared to the unsputtered surface (Fig. 2B), the amount of Ti^{3+} noticeably decreased, whereas the main Ti ($SrTiO_3$) increased to 57%, suggesting the inner material contained more $SrTiO_3$.

Comparison of the above two sintering conditions showed titanium in both the 4+ and 3+ states, but the proportion of Ti^{3+} was more in the sample reduced in N_2 atmosphere. The sputtered air-sintered surface causes an attenuation of the Ti^{3+} peaks and the appearance of a peak at 459.2 eV is assigned to the Ti^{4+} species of TiO_2. Furthermore, a peak at 461.4 eV is assigned to the corresponding Ti^{3+} ($2p_{1/2}$) level. Therefore, N_2 sintering caused a decrease of the Ti^{3+} peak intensity (3%) and a corresponding increase in the Ti^{4+} peak intensity. However, small shifts to higher binding energy (centered at 458.1 eV) of the $2p_{3/2}$ peak of Ti^{4+} of the titanate are also observed in the inner profile material.

Fig. 5C shows the XPS region around the Ti(2p) core levels for the quenched bulk obtained after Ar-sputtering. There are two peaks centered at 459.0 and 458.0 eV, assigned to the $2p_{3/2}$ core levels of TiO_2 and $SrTiO_3$, respectively. The Ti core level of the quenched inner profile material can be simulated by single Gaussians, clearly showing that no other lower valence oxidation state is detectable.

3.3. The effect of sintering temperatures

The bulks were sintered at various temperatures between 1300 and 1450 °C for two hours. The samples sintered in air at 1450 °C were bluish-gray in color, but another sample sintered below 1400 °C was buff brown in color. The samples sintered in N_2 at 1300–1450 °C were also blue in color. However, the samples quenched from high temperature were all brown. The electrical resistivity (A.C.) of the bulks measured at a frequency of 100 Hz with an LCR Analyzer are shown in Table II. Obviously, the bluish-gray samples show

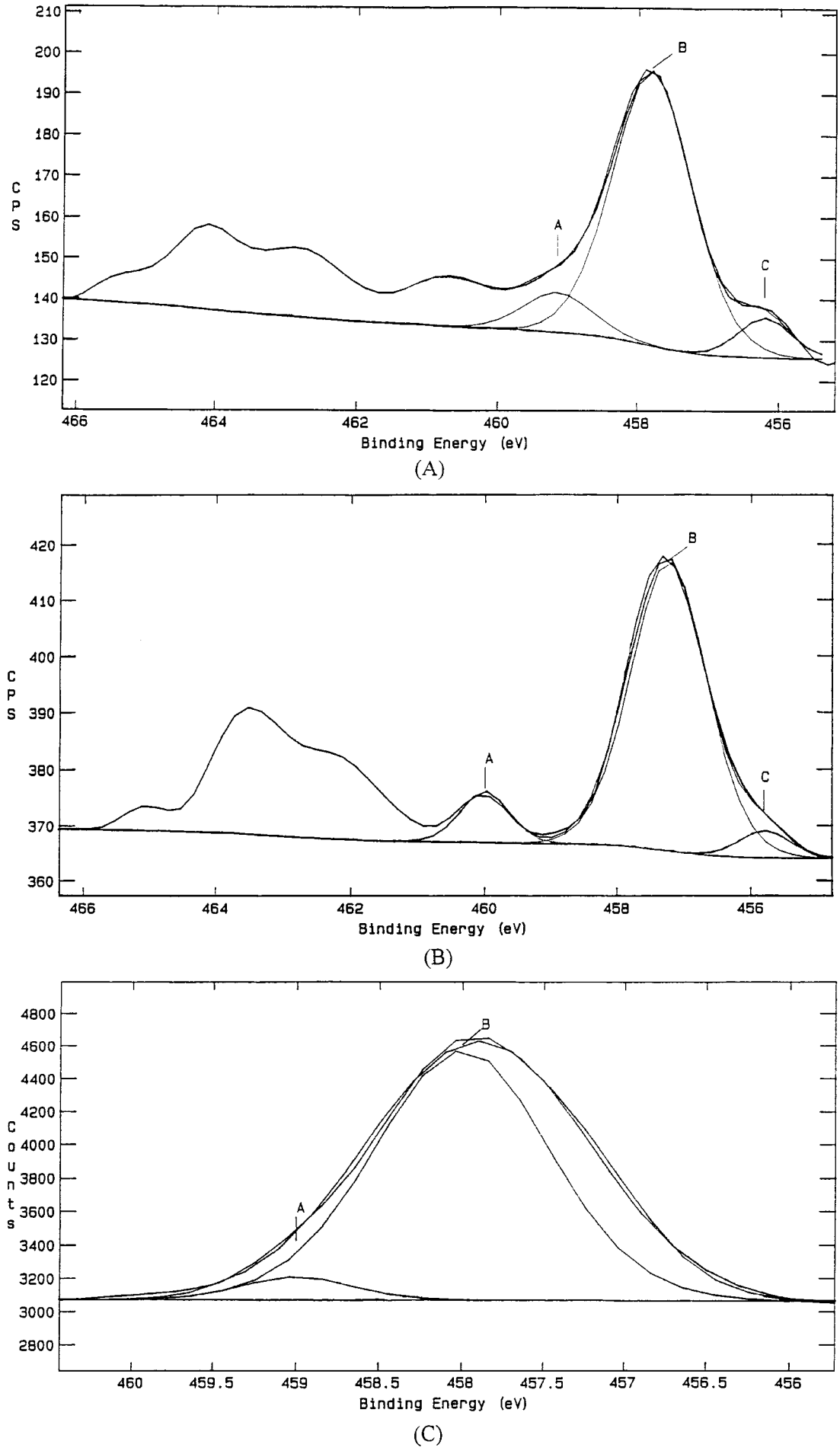

Figure 5 Ti 2p spectra for the sputtered samples: (A) sintered in air at 1450 °C for 2 h, (B) sintered in N_2 at 1450 °C for 2 h, and (C) sintered in air at 1450 °C for 2 h and quenched to room temperature.

TABLE II The A.C. electrical resistivity measured in ($\Omega \cdot$ cm) at 100 Hz of the bulks (color of sample is given in parentheses)

Sintering temperatures	1300 °C	1350 °C	1400 °C	1450 °C
Air-sintered	1.60×10^7 (brown)	1.32×10^7 (brown)	1.02×10^7 (brown)	2.47×10^6 (gray brown)
N_2-sintered	6.24×10^6 (gray blue)	1.57×10^6 (blue)	2.30×10^5 (blue)	1.12×10^5 (blue)
Quenched	2.42×10^{10} (brown)	8.41×10^9 (brown)	6.5×10^8 (brown)	8.30×10^7 (brown)

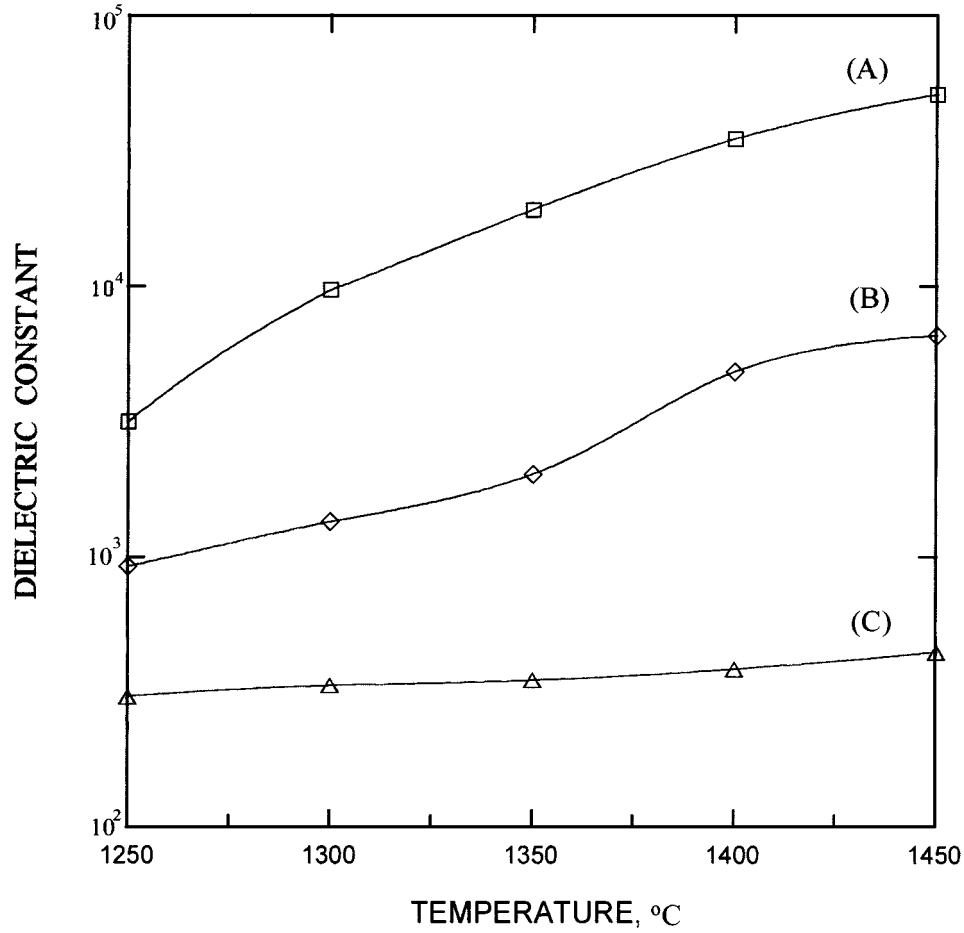

Figure 6 Dielectric constant of (La,Sr)TiO_3 bulks sintered at various temperature: (A) sintered in N_2, (B) sintered in air, and (C) the quenched bulk.

semiconducting behavior. The resistivity was about 10^4–10^6 $\Omega \cdot$ cm, for the bulks sintered in N_2 or in air at 1450 °C. Although all bulks were doped to the same extent, the quenched bulks were brown in color and had a high resistivity, about 10^8–10^{11} $\Omega \cdot$ cm. Owing to the high resistivity, the quenched bulks exhibited charge effects in the photo beams of the XPS analysis. Furthermore, after polishing the surface, the dielectric properties of the bulks were measured at a frequency of 1 kHz with an LCR Analyzer. Results are shown in Fig. 6. The N_2-sintered bulks displayed higher dielectric constants, up to 5.1×10^4 for the sample sintered at 1450 °C. Bulk (A), sintered in an air-atmosphere, lacked semiconducting behaviour, and had a lower dielectric constant than sample (B) (sintered in N_2); but the dielectric constant for the sample sintered in air at 1450 °C was anomalously large. Finally, all the bulks (C) were brown in color and highly resistant, so $SrTiO_3$ displayed a typical dielectric constant of 300–1000.

Fig. 7 shows the SEM micrographs of the ceramics sintered at 1450 °C for 2 hrs. According to Fig. 7A, the air-sintered ceramics formed a liquid phase at the grain boundary. The SEM micrograph of the N_2-sintered bulk is shown in Fig. 7B, the bulk has a similar microstructure to the bulk of Fig. 7A, but was denser. However, the ceramic obtained from the quenching process was a glassy material, less dense and showed large cavities in its microstructure. SEM suggests that the intergranular porosity of the quenched sample (Fig. 7C) is responsible for the lower dielectric constant. It also shows clearly that the glassy material at the grain boundary of this sample results in a higher brittleness as compared to $SrTiO_3$.

The XPS core levels of the samples sintered at various temperatures are shown in Fig. 8. Fig. 8A shows the sample sintered in air at 1400 °C, with binding energies at 459.6 and 457.4 eV, assigned to TiO_2 and $SrTiO_3$, respectively. No other peak at a lower energy was detected. Ti^{3+} did not exist in the bulk. Fig. 8B shows the sample sintered in N_2 at 1300 °C. Peaks at 459 and 457.6 eV, again, prove the existence of TiO_2 and $SrTiO_3$. Additionally, another peak was registered

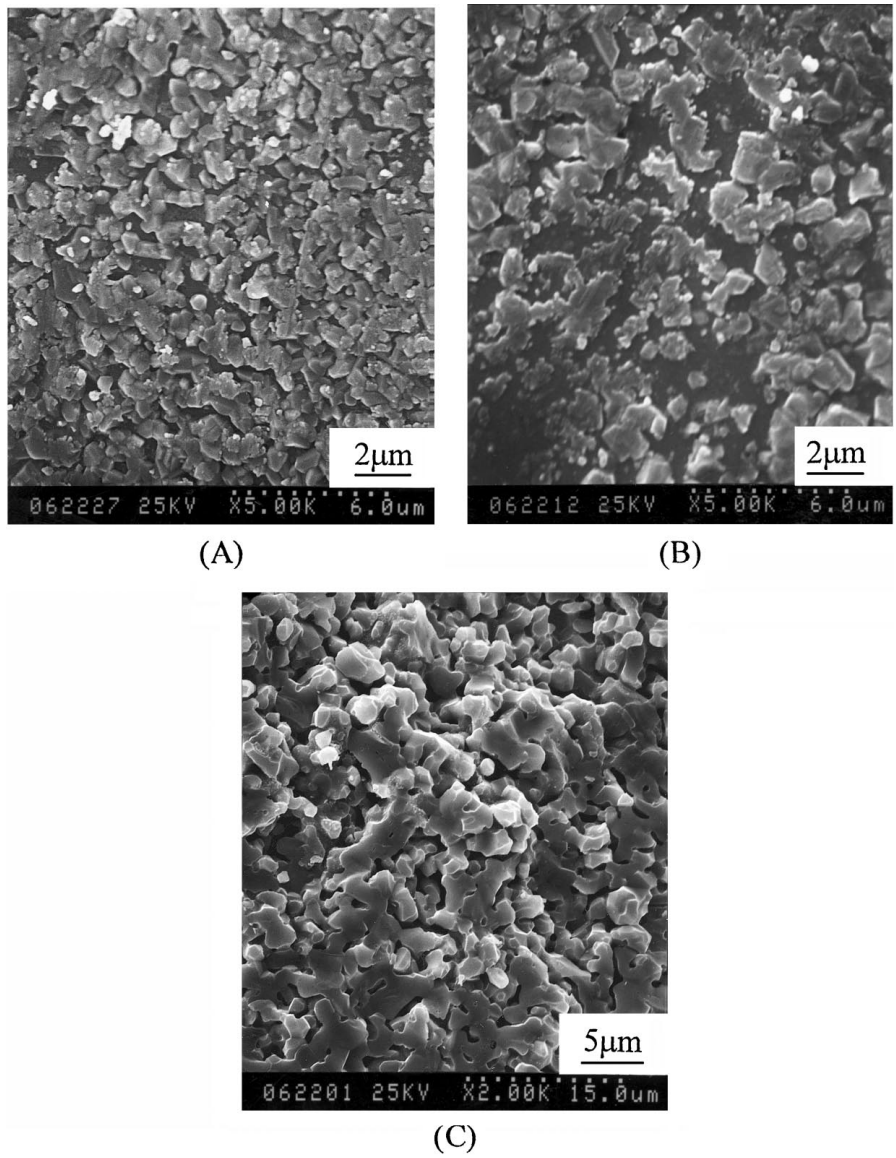

Figure 7 SEM micrographs of the bulks sintered at 1450 °C for 2 h: (A) sintered in air, (B) sintered in N_2, and (C) the quenched bulk.

at 456.9 eV, hinting at the existence of Ti^{3+}. Finally, the quenched sample (shown in Fig. 8C) sintered at 1400 °C was similar to the air-sintered sample, peaks were centered at 459 and 457.5 eV, and, as in Fig. 8A, no peak for the lower valence oxidation state titanium was detected. The Ti binding energy data of the samples are tabulated in Table III. In conclusion, combining the results from the electrical property and XPS studies it can be said that the samples sintered in air below 1400 °C do not contain Ti^{3+}, but possess a high resistivity. The bulks sintered in N_2 above 1300 °C contain considerable amounts of Ti^{3+}, which causes the bulks to have semiconducting properties and a higher dielectric constant. The quenched samples, sintered between 1300–1450 °C, contain only Ti^{4+} and the bulks are highly resistant.

The N_2-sintered or air-sintered (1450 °C) $SrTiO_3$ consists of semiconducting grains which are separated by an insulating material (Magnéli phases). The "brick-wall"-like microstructure of the Magnéli phases

TABLE III Ti binding energy data of the samples

Sample	Ti($2p_{3/2}$) TiO_2	Ti($2p_{3/2}$) $SrTiO_3$	Ti($2p_{3/2}$) Ti_2O_3	Remark
1400 °C air	459.6 [41.4%] (1.8)	457.4 [58.6%] (2.0)	—	Fig. 8A
1450 °C air	459.5 [2%] (1.0)	457.8 [90%] (1.6)	—	Fig. 2A
1300 °C N_2	459 [12.3%] (1.0)	457.6 [69%] (1.4)	456.9 [18.7%] (1.0)	Fig. 8A
1350 °C N_2	458.7 [44.7%] (0.5)	457.5 [67.6%] (1.3)	456.4 [16%] (1.1)	
1400 °C N_2	458.7 [44.7%] (2.0)	457.3 [16%] (1.8)	456.4 [39.3%] (2.0)	
1450 °C N_2	459.3 [46%] (1.8)	457.4 [36%] (1.3)	456.1 [18%] (1.2)	Fig. 2B
1400 °C quench	459.4 [18%] (1.3)	457.5 [82%] (1.5)	—	Fig. 8C
1450 °C quench	459.3 16% (1.2)	457.8 84% (1.3)	—	Fig. 2C

[ ]: mol %; ( ): FWHM.

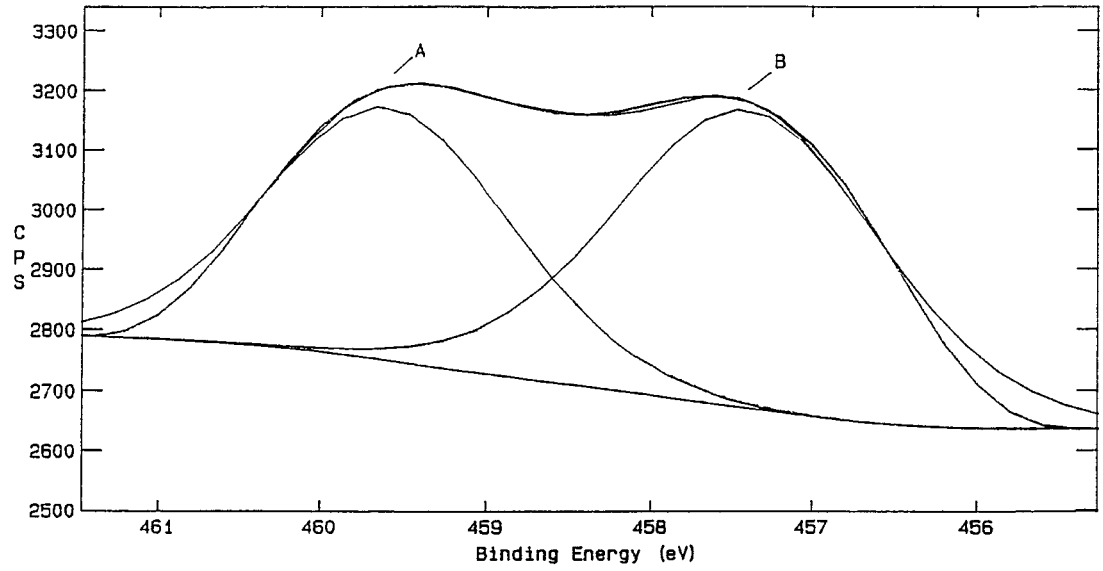

(A)

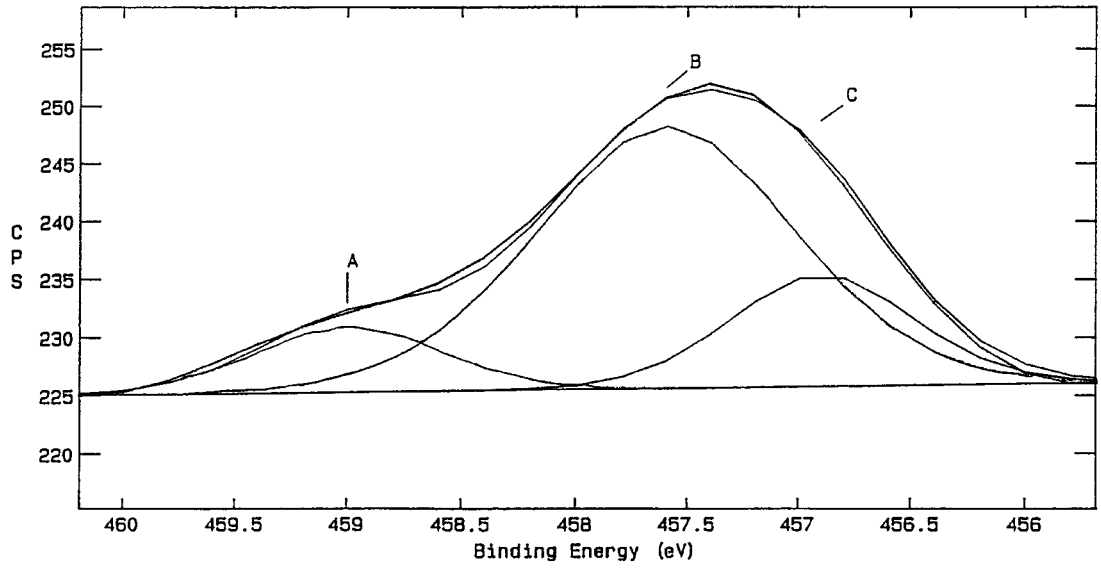

(B)

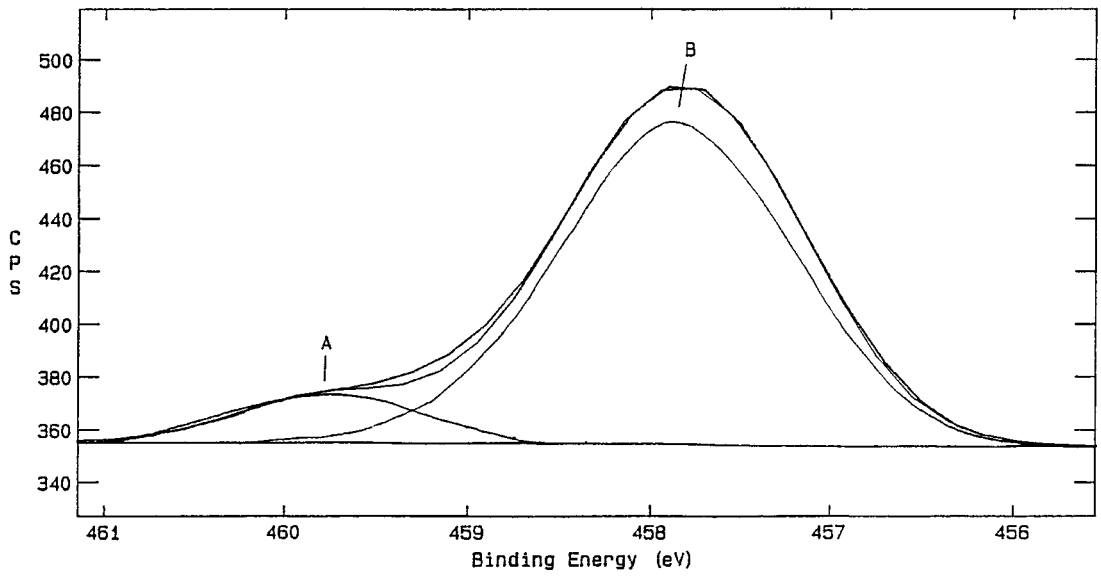

(C)

Figure 8 The Ti core levels of XPS of samples sintered at various conditions: (A) the sample sintered in air at 1450 °C, (B) the sample sintered in N_2 at 1300 °C, and (C) the quenched sample sintered at 1400 °C.

surrounds the $SrTiO_3$ grain, resulting in a have a high dielectric constant [30].

4. Conclusions

By chelating titanium alkoxide with acetic acid through the sol-precipitation process, highly dense strontium titanate ceramics were obtained after sintering the ultrafine powders. X-ray photoelectron spectroscopy was used to investigate the La_2O_3-doped $SrTiO_3$ surface to reveal the surface compositions and investigate the existence of Ti^{3+}, which is responsible for the semiconducting properties. The surfaces were found to have Sr/Ti ratios varying significantly from the stoichiometric ratio. Carbon contamination of the surface was revealed and suggested the presence of hydroxyl groups on the surface, which largely decreased in side the bulk. Ti^{3+}, in the form of Ti_2O_3 has been monitored as a function of the sintering conditions, and could be detected at the surface of $(La,Sr)TiO_3$ sintered in either air or in N_2 and cooled naturally. Ti^{3+} was present, especially when the samples were sintered in N_2 atmosphere. Finally, the quenched samples had a high resistivity, and clearly showed a glassy material at the grain boundary, resulting in brittleness. Noticeable amounts of Ti^{3+} were not detected in these samples.

The resistivity of the bulks decreased with an increase of the Ti^{3+}-surface concentration, leading to semiconductivity of the samples. Out of the air-sintered samples, only the one sintered at 1450 °C was deeply blue-gray in color and exhibited a relatively low resistivity, owing to the presence of Ti^{3+} on its surface. The N_2-sintered samples also had a low resistivity when sintered above 1350 °C. They were dark blue in color and semiconducting, which again was due to the presence of lower valence oxidation state Ti detected by the XPS surface analysis.

References

1. J. M. WILSON and D. L. COLLER, U. S. Patent no. 4,670,243 (1987).
2. P. P. PHULE and S. H. RISBUD, *Mater. Sci. Eng. B* **3** (1989) 241.
3. C. F. KAO and W. D. YANG, *Ceramics International* **22** (1996) 57.
4. F. CHAPUT and J. P. BOILOT, *J. Mater. Sci. Lett.* **6** (1987) 1120.
5. C. F. KAO and W. D. YANG, *Mater. Sci. Eng. B* **B38** (1996) 127.
6. P. E. C. FRANKEN, *J. Amer. Ceram. Soc.* **64** (1981) 687.
7. D. E. RASE and R. ROY, *ibid.* **38** (1955) 102.
8. S. WAKU, *N. T. T. Res. Appl. Rept.* **16** (1967) 975.
9. A. G. SARKISYAN, V. M. ARUTYUNYAN, V. E. MELIKYAN and E. V. PUTNYN, *Elektrokhimiya* **22** (1986) 511.
10. B. T. CHANG, *Solid State Comm.* **43** (1982) 335.
11. T. R. N. AVUDAITHAI, *Mater. Res. Bull.* **25** (1990) 821.
12. A. MACKOR and G. BLASSE, *Chem. Phys. Lett.* **77** (1981) 6.
13. N. H. CHAN, R. K. SHARMA and D. M. SMYTH, *J. Electrochem. Soc.* **128** (1981) 1762.
14. H. P. R. FREDERIKSE and W. R. HOSLER, *Phys. Rev.* **155** (1967) 796.
15. U. BALACHANDRAN and N. G. EROR, *J. Electrochem. Soc.: Solid-State Science and Technology* **129** (1982) 1021.
16. V. E. HENRICH, *Rep. Prog. Phys.* **48** (1985) 1481.
17. S. FERRER and G. A. SOMORJAI, *Surface Science* **94** (1980) 41.
18. P. V. NAGARKAR, P. C. SEARSON and F. D. GEALY, III, *J. Appl. Phys.* **69** (1991) 459.
19. A. F. CARLEY, P. R. CHALKER, J. C. RIVIERE and M. W. ROBERTS, *J. Chem. Soc., Faraday Trans. I* **83** (1987) 351.
20. C. F. KAO and W. D. YANG, *Mater. Trans. JIM* **37** (1996) 142.
21. V. YOUNG and T. OTAGAWA, *Appl. Surf. Sci.* **20** (1985) 228.
22. N. R. ARMSTRONG and R. K. QUINN, *Surface Science* **67** (1977) 451.
23. M. E. LEVIN, M. SALMERON, A. T. BELL and G. A. SOMORJAI, *ibid.* **195** (1988) 429.
24. R. P. VASQUEZ, *J. Electron Spectrosc.* **56** (1991) 217.
25. M. E. PILLEUX, C. R. GRAHMANN and V. M. FUENZALIDA, *J. Amer. Ceram. Soc.* **77** (1994) 1601.
26. S. MYHRA, J. C. RIVIERE, K. HAWKINS and T. J. WHITE, *J. Mater. Res.* **7** (1992) 482.
27. D. S. KNOTEK and R. M. GLAISTER, *Proc. Inst. Electr. Eng. Part B* **109** (1961) 423.
28. M. FUJIMOTO and M. WATANABE, *J. Mater. Sci.* **20** (1985) 2683.
29. G. ROCKER and W. GOPEL, *Surface Science* **18** (1987) 530.
30. M. V. RAYMOND and V. R. W. AMARAKOON, *J. Amer. Ceram. Soc.* **73** (1990) 1308.

Received 19 August 1997
and accepted 27 January 1999